

Amphoteric Be in GaN: Experimental Evidence for Switching between Substitutional and Interstitial Lattice Sites

Filip Tuomisto,¹ Vera Prozheeva,¹ Ilja Makkonen,¹ Thomas H. Myers,² Michal Bockowski,³ and Henryk Teisseyre⁴

¹Department of Applied Physics, Aalto University, P.O. Box 15100, FI-00076 Aalto, Espoo, Finland

²Materials Science, Engineering, and Commercialization Program, Texas State University,
601 University Drive, San Marcos, Texas 78666, USA

³Institute of High Pressure Physics PAS, Sokotowska 29/37, 01-142 Warsaw, Poland

⁴Institute of Physics PAS, Al. Lotników 32/46, 02-668 Warsaw, Poland

(Received 28 June 2017; published 9 November 2017)

We show that Be exhibits amphoteric behavior in GaN, involving switching between substitutional and interstitial positions in the lattice. This behavior is observed through the dominance of Be_{Ga} in the positron annihilation signals in Be-doped GaN, while the emergence of V_{Ga} at high temperatures is a consequence of the Be impurities being driven to interstitial positions. The similarity of this behavior to that found for Na and Li in ZnO suggests that this could be a universal property of light dopants substituting for heavy cations in compound semiconductors.

DOI: 10.1103/PhysRevLett.119.196404

The quest for efficient *p*-type dopants in wide band gap compound semiconductors, such as GaN and ZnO, has been long and largely unsuccessful. Approaches adopted from semiconductor technology based on Si and GaAs, where suitable donors and acceptors with low activation energies are found in the periodic table right next to the atoms constituting the host lattice, have essentially failed. For example, the state-of-the-art choice for *p*-type doping of GaN is Mg, a light alkaline earth metal, whose activation efficiency is only about 1%. Remarkably, even though Mg has already been utilized as *the p*-type dopant in GaN devices for decades, both the exact lattice location and electronic activity of this impurity are still debated [1–4]. The relatively high activation energy and passivation-compensation issues result in poor activation of Mg—better *p*-type dopants would clearly be welcome.

Interest in Be as a dopant in GaN has recently reemerged thanks to the appearance of encouraging reports from experimental activities [5–9] and novel predictions with improved theoretical methods [10]. While *p*-type GaN may not be achieved with Be doping, semi-insulating material is highly desirable for manufacturing high-electron-mobility transistors, for example. The dominant lattice locations and related optical signatures [7,9], particularly self-compensation through the balance between substitutional and interstitial positions [10], need to be understood in detail for efficient use of Be in GaN-based devices.

In this Letter, we show that Be impurities exhibit amphoteric behavior in GaN, similar to what has been found for Li impurities in ZnO [11,12] and for certain vacancy-type defects in III-V semiconductors [13,14]. This finding suggests a universal property of small elements substituting for large cation atoms in these compounds, that is, the rise of a competition between substitutional and interstitial lattice

sites. We arrived at these conclusions by performing positron annihilation spectroscopy [15] on Be-doped GaN thin films grown by molecular beam epitaxy (MBE) and bulk crystals grown by the high nitrogen pressure solution (HNPS) method. Our experimental approach is augmented by state-of-the-art modeling of positron states and annihilation signals. In addition, positrons can provide detailed information on small substitutional elements [12].

The Be-doped GaN MBE thin films were grown at 675–770 °C on GaN templates (Ga-polar samples) or directly on sapphire substrates (N-polar samples) [16]. Postgrowth heat treatments were performed on the Ga-polar samples in N₂ ambient at a temperature of 900 °C for 2 h. The growth conditions were similar for all the thin films, except for the sample N2 where the Ga flux was significantly lower (9 vs 16 × 10⁻⁷ Torr). The Ga-polar samples were found to be semi-insulating before and after postgrowth heat treatment, except for Ga5 (as-grown) exhibiting *n*-type behavior. The crystallization processes of the HNPS bulk crystals are described in Refs. [7,17]. Be concentrations were determined by secondary ion mass spectrometry. Table I summarizes the impurity concentrations and the relative *S* and *W* Doppler broadening parameters (reference: *p*-type GaN) in the samples.

We performed both conventional and coincidence Doppler broadening measurements of positron annihilation radiation with a variable-energy positron beam. We used high purity germanium (HPGe) detectors with an energy resolution of 1.2 keV at 511 keV. The integration windows for the *S* and *W* parameters were set to $|p_L| < 0.4$ a.u. and $1.6 \text{ a.u.} < |p_L| < 4.0 \text{ a.u.}$, respectively. We performed positron lifetime experiments on the HNPS GaN samples with a standard temperature-controlled digital spectrometer in collinear geometry and time resolution of 250 ps

TABLE I. Be content and relative (S, W) parameters for the Be-doped GaN samples. Samples Ga1–Ga5 are Ga-polar and N1–N3 are N-polar thin films. “A” stands for annealed. HNPS low-O is a low-oxygen bulk crystal with $[O] \sim 10^{19} \text{ cm}^{-3}$. The samples that do not follow the general trends discussed in the text are marked with *.

Sample	[Be] (cm^{-3})	S relative	W relative
Ga1	5×10^{17}	1.000(2)	0.961(7)
Ga1A*	5×10^{17}	1.002(2)	0.950(7)
Ga2	1×10^{18}	0.997(2)	0.963(7)
Ga2A	1×10^{18}	1.008(2)	0.919(7)
Ga3	2×10^{18}	0.996(2)	0.969(7)
Ga3A	2×10^{18}	1.008(2)	0.917(7)
Ga4	4×10^{18}	0.996(2)	0.967(7)
Ga4A	4×10^{18}	1.007(2)	0.904(7)
Ga5	1×10^{19}	1.003(2)	0.942(7)
Ga5A	1×10^{19}	1.006(2)	0.908(7)
N1	7×10^{18}	0.999(2)	0.959(7)
N2*	7×10^{18}	1.013(2)	0.921(7)
N3	7×10^{18}	1.003(2)	0.938(7)
HNPS low-O	3×10^{19}	1.008(3)	0.92(1)

(FWHM). More details on the experimental techniques and data analysis can be found in Ref. [15].

We used *ab initio* electronic structure calculations to model the positron annihilation parameters in the GaN lattice and at different kinds of relaxed defect structures, taking into account the forces exerted on the ions by the localized positron [18]. The valence electron densities were obtained self-consistently via the local-density approximation (LDA), employing the projector augmented-wave (PAW) method [19] and the plane-wave code VASP [20]. The positron states and annihilation characteristics were determined using the LDA [21] and the state-dependent scheme [22] for the momentum densities of annihilating electron-positron pairs. We use a 96-atom GaN wurtzite supercell and check the positron localization to substitutional Be_{Ga} with a 768-atom cell. The Doppler spectra were computed using reconstructed PAW orbitals [18] and atomic orbitals for the core electrons, and finally convoluted with the experimental resolution.

Figure 1 presents the S parameter measured in selected samples as a function of positron implantation energy and corresponding positron implantation depth. The region of the roughly constant S parameter is different from sample to sample due to the different thickness of the GaN:Be layer in each sample, and extends from about 5 keV up to 15 keV in the thickest samples. The data obtained at these energies can be taken as characteristic of the layer. The increased S parameter in the annealed layers compared to the defect-free p -type GaN reference sample indicates that the positron-electron momentum distribution is narrower in these samples. This is a clear sign of vacancy defects present in the measured layers. Interestingly, the S parameter in most

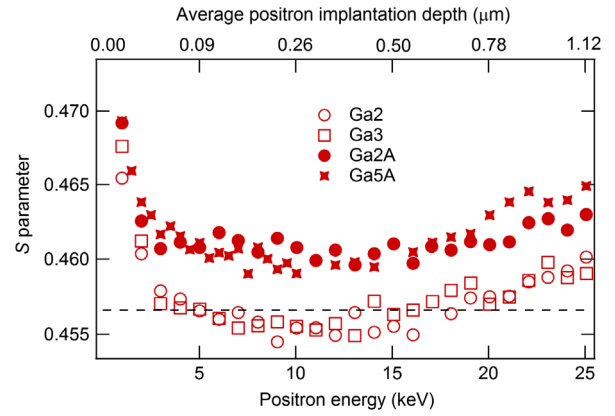


FIG. 1. The S parameter measured as a function of positron implantation energy (implantation depth) in selected MBE-grown Be-doped GaN thin films before and after annealing. The dashed line corresponds to the bulk S parameter value of the p -type GaN reference.

of the as-grown layers is very close to or even lower than that measured in the reference sample, indicating that either the as-grown samples have very low vacancy-type defect concentration or that positron annihilation is observed at nontypical vacancy defects.

Figure 2 shows the (S, W) points for each sample, obtained by averaging over the layer thickness with constant (S, W) values for the thin films, and over the high implantation energy region values for the bulk crystal. The error bars denote the statistical deviation within the selected positron implantation energy range. The data are normalized to those of the p -type GaN reference sample. The experimentally determined (S, W) point characteristic of the isolated V_{Ga} is denoted by “ V_{Ga} exp.” This point and its error bars have been determined by remeasuring and combining [23] the data from electron-irradiated samples [24], He^+ ion-irradiated samples [25], and H^+ ion-implanted samples [26]. In addition to the experimental data, the figure shows theoretically calculated (S, W) points and positron lifetimes for defects related to V_{Ga} and Be_{Ga} . We included Be_{Ga} -related defects because earlier findings [12] on Li_{Zn} in ZnO found that despite its small associated open volume, Li_{Zn} still acts as an efficient positron trap. Indeed our theoretical calculations predict positron localization at Be_{Ga} in GaN. We performed the calculations for neutral and negative charge states of Be_{Ga} : the differences in the original atomic configurations are insignificant from the point of view of the positron signals due to the relaxations produced by the positron localized in the defect. Importantly, the calculated data points for V_{Ga} complexed with oxygen or a single hydrogen atom are very hard to distinguish from each other and from the isolated V_{Ga} , as found in earlier experimental and theoretical work [24,27].

The data points of the Be-doped GaN samples do not fall on the line connecting the GaN lattice to V_{Ga} nor above it (nor to the right of it), as would be typical of GaN containing

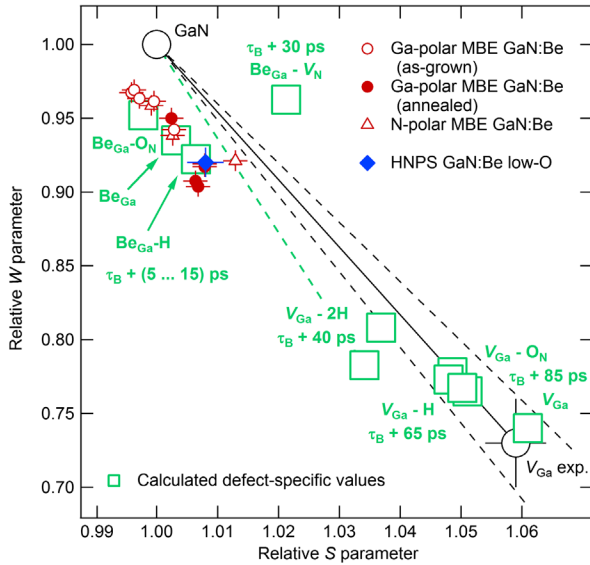


FIG. 2. Relative (S, W) parameters measured in Be-doped GaN. Theoretically calculated parameters for a variety of defects are shown in addition to the experimentally determined (S, W) parameters typical of isolated Ga vacancies in GaN. The calculated effect of V_{Ga} complexed with one or more nitrogen vacancies (not shown for the sake of clarity) is consistent with Ref. [27]; i.e., the data points have a similar W and clearly higher S than V_{Ga} . We also show the theoretically calculated positron lifetime values for the defects, relative to the GaN lattice lifetime τ_B . A single lifetime is shown for defects with similar calculated lifetime values, such as the different configurations of $V_{\text{Ga}}\text{-O}_N$ and V_{Ga} , or the different Be_{Ga} complexes. The calculations were performed for two different configurations for each of the V_{Ga} complexes.

either in-grown or processing-induced V_{Ga} -related defects [28–30]. Instead, all the data points from the Be-doped samples are located in the vicinity of the calculated points for Be_{Ga} -related defects. These observations strongly suggest that the defects detected by positrons in Be-doped GaN are of Be_{Ga} nature. The data points from the as-grown Be-doped GaN thin films are clustered towards the upper left, while the data points from the annealed samples are clustered towards the lower right with the data point obtained in the Be-doped GaN bulk crystal (low-O). The samples Ga1A and N2 do not follow the general trend. Yet the point for Ga1A is towards the lower right from Ga1, while the growth conditions for N2 were different compared to the rest of the thin films.

Figure 3 displays ratio curves: coincidence Doppler broadening spectra for representative as-grown and annealed Ga-polar thin film samples normalized to those obtained in the p -type GaN reference. As has been shown, the comparison of experimental and theoretical ratio curves is an exceptionally valuable tool in defect identification, with excellent matches for cation vacancy defects in GaN, InN and oxide semiconductors [24,30]. Theoretically calculated ratio curves for Be_{Ga} , $\text{Be}_{\text{Ga}}\text{-H}$, $\text{Be}_{\text{Ga}}\text{-V}_N$, $\text{Be}_{\text{Ga}}\text{-O}_N$, V_{Ga} , and $V_{\text{Ga}}\text{-2H}$ are also presented in Fig. 3. The most important

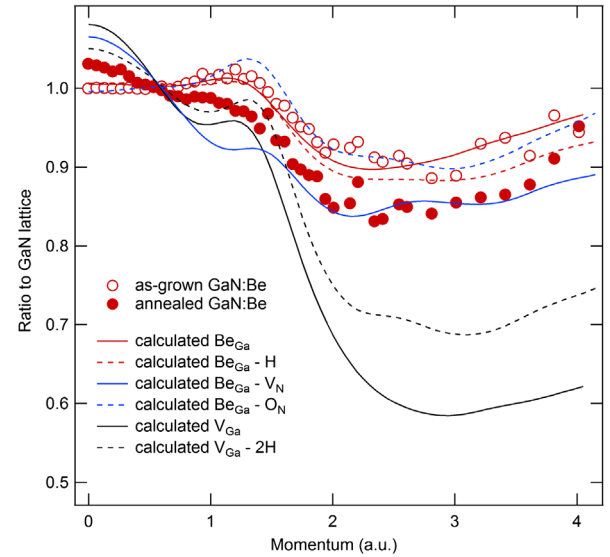


FIG. 3. Ratio curves obtained from coincidence Doppler broadening experiments in Ga-polar samples and from theoretical calculations. The comparison of experimental and theoretical data clearly shows that defects related to Be_{Ga} are detected in Be-doped GaN.

features in these curves, in order of importance, are the intensity close to 0 a.u. (the S -parameter region), the intensity above 2 a.u. (the W -parameter region), the relationship between these two intensities, and the shoulderlike feature in the range of 1–2 a.u. [15]. It is clear that the defects observed in the as-grown sample are related to Be_{Ga} , $\text{Be}_{\text{Ga}}\text{-H}$ or $\text{Be}_{\text{Ga}}\text{-O}_N$, as the ratio curves for all the other defects are notably different. After annealing, the positron data obtained in the Be-doped samples are clearly affected by V_{Ga} -related defects, while still resembling the Be_{Ga} signals. Importantly, there is no evidence for the presence of Be_{Ga} complexed with nitrogen vacancies, as seen also in Fig. 2 where the point characteristic of the $\text{Be}_{\text{Ga}}\text{-V}_N$ complex is far to the right from the experimental data.

Through positron lifetime experiments in HNPS-grown GaN:Be bulk crystals, we have further verified our interpretation of substitutional Be_{Ga} acting as an efficient positron trap in GaN. Figure 4 shows the average positron lifetime measured as a function of temperature in two different crystals. One is a high-oxygen ($\sim 10^{20} \text{ cm}^{-3}$) crystal already studied earlier [31], and the other is a state-of-the-art low-oxygen ($\sim 10^{19} \text{ cm}^{-3}$) crystal [7]. The figure also shows the data from a highly Mg-doped ammonothermally grown GaN crystal that provides the values characterizing the GaN lattice [32]. The Be-doped crystals show a 5–10 ps longer single lifetime than in the GaN lattice at temperatures below 300 K. The high-O HNPS GaN clearly also contains Ga vacancy-related defects that become visible at temperatures above 300 K, as seen through the emergence of the second lifetime component of about 230 ps (Fig. 4 top). The theoretical predictions for

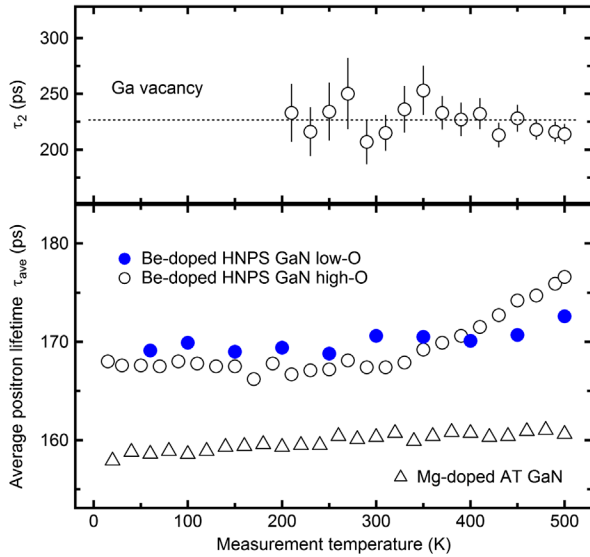


FIG. 4. Average positron lifetimes (bottom) extracted from the lifetime spectra measured in the low-O HNPS-grown bulk GaN as a function of measurement temperature. The data obtained in Mg- and high-O Be-doped GaN (also the second lifetime component, top) from earlier experiments [31,32] are shown for comparison.

the Be_{Ga} -related defects (Fig. 2) match the experimental observation and also rule out the $\text{Be}_{\text{Ga}} - V_{\text{N}}$ complexes.

Our data show that positron annihilation is dominated by Be_{Ga} -related defects in all the as-grown Ga-polar Be-doped MBE-grown thin films, in the N-polar samples N1 and N3, and in the Be-doped HNPS GaN low-O bulk crystal. The strength of the signal implies that the concentration of these defects is at least in the 10^{17} cm^{-3} range, consistent with the lowest Be doping. In addition to the Be_{Ga} signal, V_{Ga} -type defects produce a significant signal in the annealed Ga-polar samples, in the N-polar sample N2, and in the Be-doped HNPS GaN high-O single crystal. Generally, doping with Be makes GaN semi-insulating, as is the case with the present samples as well. The associated relatively low-lying Fermi level makes the thermal formation of acceptorlike V_{Ga} very unlikely due to their high formation energy [33,34]. Hence the nonobservation of V_{Ga} in most of the as-grown MBE samples comes as little surprise. The sample N2 was grown at a significantly lower Ga flux, explaining the presence of a V_{Ga} -related signal in this sample. The observation of significant concentrations of V_{Ga} -related defects in MBE thin films after thermal annealing at 900°C and in the high-O HNPS bulk crystal calls for further consideration.

Efficient generation of acceptor-type V_{Ga} can proceed either through the direct mechanism of $\text{Be}_{\text{Ga}} \rightarrow V_{\text{Ga}} + \text{Be}_i$ or indirectly through thermal vacancy formation if the Fermi level is sufficiently close to the conduction band minimum during the heat treatment. The latter mechanism also requires that Be impurities are efficiently excited from the substitutional to interstitial positions, since Be_{Ga} are acceptors but Be_i are double donors [10]. Hence, the presence of V_{Ga}

after annealing is an indication of Be switching between substitutional and interstitial sites. As the samples are semi-insulating after the heat treatment, most of the Be impurities regain their substitutional position during cooling. It should be noted that with the present Be concentrations, it is sufficient that only a small fraction, of the order of 10%, of Be_i are not converted back to Be_{Ga} during cooling for the V_{Ga} concentration to have the effect on the positron data observed in Fig. 3. The emergence of the V_{Ga} -related defects after annealing explains the appearance of additional donor-acceptor pair photoluminescence signatures found in the MBE-grown Be-doped thin films [16].

The estimation of V_{Ga} equilibrium concentration provides further insight into the defect formation mechanism. The formation energy of triple acceptor V_{Ga} has been determined [35] to be $E^f = 3.0 \pm 0.5 \text{ eV}$ at the Fermi level position $E_C - E_F = 0.5 \text{ eV}$, corresponding to $E^f = 1.5 \pm 0.5 \text{ eV}$ when the Fermi level E_F coincides with the conduction band minimum E_C . Assuming a formation entropy of $S = 5 \dots 10 k_B$, the upper limit of the equilibrium concentration of V_{Ga} at a temperature of 900°C can be estimated as $3 \times 10^{16} \text{ cm}^{-3}$. For the V_{Ga} -type signal to be significant after annealing, the concentration of the thermally generated V_{Ga} must be of the same order of magnitude as that of Be_{Ga} , that is, mid- 10^{17} cm^{-3} or above. Hence, the direct mechanism ($\text{Be}_{\text{Ga}} \rightarrow V_{\text{Ga}} + \text{Be}_i$) is the more likely process behind the V_{Ga} generation during annealing of the thin films. For this process to be important after 2 h at 900°C but inefficient at 700°C (the growth temperature), the activation energy can be estimated as $E_A = 3.5 \pm 0.5 \text{ eV}$.

The amphoteric behavior of Be, involving switching from a substitutional to an interstitial position, also explains the data in the HNPS bulk crystals that are grown at much higher temperatures than the MBE thin films. Both in the high-O and low-O cases, the Be impurities are substitutional at low temperatures and interstitial at high temperatures, thus promoting V_{Ga} formation. However, only in the high-O case do the Ga vacancies survive the cooling from the growth temperature through efficient formation of complexes with O [35]. This is in excellent agreement with the recent results obtained by combining pressure-dependent photoluminescence experiments with theoretical calculations, showing the dominance of Be_{Ga} and $\text{Be}_{\text{Ga}}-\text{O}_{\text{N}}$ -related optical signatures in the low-O HNPS bulk crystals [36]. The concentration of V_{Ga} -related defects was found to correlate with the Be concentration; adding Be to the growth environment promotes V_{Ga} formation even with the presence of a very high Be concentration [31,37]. This finding reveals a rather surprising difference between Mg and Be acceptors in GaN: while high Mg doping prevents Ga vacancy formation, Be at high enough concentrations and temperatures promotes it [38]. In addition, most of the Be must be in substitutional sites after cooling to passivate the donor character of the O impurities, furthering evidence for switching between substitutional and interstitial sites working in both directions. Remarkably, similar thermal

and Fermi-level dependent competition between substitutional and interstitial sites has also been observed for Na and Li in ZnO [39,40]. Metal-substituting light atom dopants have also been suggested to exhibit similarities in their electronic properties in GaN and ZnO [4].

In summary, we show that Be exhibits amphoteric behavior in GaN, involving switching between substitutional (acceptor) and interstitial (donor) positions in the lattice. This is observed through the dominance of Be_{Ga} in the positron annihilation signals in Be-doped GaN. Subjecting the material to high enough temperatures drives the Be impurities to interstitial positions, observed through the emergence of V_{Ga} -related defects in concentrations comparable to those of Be_{Ga} . The thermal switching between interstitial and substitutional sites of Be appears reversible, as Be-doped GaN is predominantly semi-insulating before and after subjection to high temperatures. We suggest this behavior to be a universal property of light atom dopants substituting for heavy cations in compound semiconductors.

We acknowledge the computational resources provided by the Aalto Science-IT project and CSC—Finnish IT Centre for Science. This work was partially supported by the Academy of Finland Grants No. 277193, No. 285809, and No. 293932, and by the Polish National Science Centre Grant No. DEC-2011/03/B/ST3/02647. We thank A. Karjalainen for technical assistance with the experiments.

-
- [1] U. Wahl *et al.*, *Phys. Rev. Lett.* **118**, 095501 (2017).
 [2] J. Buckeridge, C. R. A. Catlow, D. O. Scanlon, T. W. Keal, P. Sherwood, M. Miskufova, A. Walsh, S. M. Woodley, and A. A. Sokol, *Phys. Rev. Lett.* **114**, 016405 (2015).
 [3] J. L. Lyons, A. Janotti, and C. G. Van de Walle, *Phys. Rev. Lett.* **108**, 156403 (2012).
 [4] S. Lany and A. Zunger, *Appl. Phys. Lett.* **96**, 142114 (2010).
 [5] D. F. Storm, D. S. Katzer, S. C. Binari, E. R. Glaser, B. V. Shanabrook, and J. A. Roussos, *Appl. Phys. Lett.* **81**, 3819 (2002).
 [6] E. R. Glaser, J. A. Freitas, D. F. Storm, H. Teisseyre, and M. Boćkowski, *J. Cryst. Growth* **403**, 119 (2014).
 [7] H. Teisseyre, M. Bockowski, I. Grzegory, A. Kozanecki, B. Damilano, Y. Zhydachevskii, M. Kunzer, K. Holc, and U. T. Schwarz, *Appl. Phys. Lett.* **103**, 011107 (2013).
 [8] J. Dashdorj, M. E. Zvanut, and M. Bockowski, *Phys. Status Solidi (b)* **252**, 923 (2015).
 [9] W. R. Willoughby, M. E. Zvanut, J. Dashdorj, and M. Bockowski, *J. Appl. Phys.* **120**, 115701 (2016).
 [10] J. L. Lyons, A. Janotti, and C. G. Van de Walle, *Jpn. J. Appl. Phys.* **52**, 08JJ04 (2013).
 [11] S. Lany and A. Zunger, *Phys. Rev. B* **80**, 085202 (2009).
 [12] K. M. Johansen, A. Zubiaga, I. Makkonen, F. Tuomisto, P. T. Neuvonen, K. E. Knutsen, E. V. Monakhov, A. Yu. Kuznetsov, and B. G. Svensson, *Phys. Rev. B* **83**, 245208 (2011).
 [13] W. Walukiewicz, *Appl. Phys. Lett.* **54**, 2094 (1989).
 [14] N. Segercrantz, J. Slotte, F. Tuomisto, K. Mizohata, and J. Räisänen, *Phys. Rev. B* **95**, 184103 (2017).
 [15] F. Tuomisto and I. Makkonen, *Rev. Mod. Phys.* **85**, 1583 (2013).
 [16] K. Lee, B. L. VanMil, M. Luo, L. Wang, N. C. Giles, and T. H. Myers, *Phys. Status Solidi (c)* **2**, 2204 (2005).
 [17] M. Bockowski *et al.*, *Technology of Gallium Nitride Crystal Growth* (Springer Verlag, Berlin, 2010), Chap. 10.
 [18] I. Makkonen, M. Hakala, and M. J. Puska, *Phys. Rev. B* **73**, 035103 (2006); *J. Phys. Chem. Solids* **66**, 1128 (2005).
 [19] P. E. Blöchl, *Phys. Rev. B* **50**, 17953 (1994).
 [20] G. Kresse and J. Furthmüller, *Phys. Rev. B* **54**, 11169 (1996); *Comput. Mater. Sci.* **6**, 15 (1996); G. Kresse and D. Joubert, *Phys. Rev. B* **59**, 1758 (1999).
 [21] E. Boroński and R. M. Nieminen, *Phys. Rev. B* **34**, 3820 (1986).
 [22] M. Alatalo, B. Barbiellini, M. Hakala, H. Kauppinen, T. Korhonen, M. J. Puska, K. Saarinen, P. Hautojärvi, and R. M. Nieminen, *Phys. Rev. B* **54**, 2397 (1996).
 [23] F. Linez, I. Makkonen, and F. Tuomisto, *Phys. Rev. B* **94**, 014103 (2016).
 [24] S. Hautakangas, I. Makkonen, V. Ranki, M. J. Puska, K. Saarinen, X. Xu, and D. C. Look, *Phys. Rev. B* **73**, 193301 (2006).
 [25] F. Tuomisto, A. Pelli, K. M. Yu, W. Walukiewicz, and W. J. Schaff, *Phys. Rev. B* **75**, 193201 (2007).
 [26] F. Tuomisto, *Appl. Surf. Sci.* **255**, 54 (2008).
 [27] S. Ishibashi and A. Uedono, *J. Phys. Conf. Ser.* **505**, 012010 (2014).
 [28] F. Tuomisto, T. Paskova, S. Figge, D. Hommel, and B. Monemar, *J. Cryst. Growth* **300**, 251 (2007).
 [29] H. Nykänen, S. Suihkonen, L. Kilanski, M. Sopanen, and F. Tuomisto, *Appl. Phys. Lett.* **100**, 122105 (2012).
 [30] A. Uedono, S. Ishibashi, K. Tenjinbayashi, T. Tsutsui, K. Nakahara, D. Takamizu, and S. F. Chichibu, *J. Appl. Phys.* **111**, 014508 (2012); C. Rauch, I. Makkonen, and F. Tuomisto, *Phys. Rev. B* **84**, 125201 (2011); I. Makkonen, E. Korhonen, V. Prozheeva, and F. Tuomisto, *J. Phys. Condens. Matter* **28**, 224002 (2016).
 [31] K. Saarinen, V. Ranki, T. Suski, M. Bockowski, and I. Grzegory, *J. Cryst. Growth* **246**, 281 (2002).
 [32] F. Tuomisto, J.-M. Mäki, and M. Zajac, *J. Cryst. Growth* **312**, 2620 (2010).
 [33] S. Limpijumng and C. G. Van de Walle, *Phys. Rev. B* **69**, 035207 (2004).
 [34] C. G. Van de Walle, S. Limpijumng, and J. Neugebauer, *Phys. Rev. B* **63**, 245205 (2001).
 [35] F. Tuomisto, K. Saarinen, T. Paskova, B. Monemar, M. Bockowski, and T. Suski, *J. Appl. Phys.* **99**, 066105 (2006).
 [36] H. Teisseyre, J. L. Lyons, A. Kaminska, D. Jankowski, D. Jarosz, M. Bockowski, A. Suchocki, and C. G. Van de Walle, *J. Phys. D: Appl. Phys.* **50**, 22LT03 (2017).
 [37] J. Oila *et al.*, *Phys. Rev. B* **63**, 045205 (2001).
 [38] F. B. Naranjo *et al.*, *Phys. Status Solidi (a)* **180**, 97 (2000).
 [39] P. T. Neuvonen, L. Vines, V. Venkatachalapathy, A. Zubiaga, F. Tuomisto, A. Hallén, B. G. Svensson, and A. Yu. Kuznetsov, *Phys. Rev. B* **84**, 205202 (2011).
 [40] P. T. Neuvonen, L. Vines, B. G. Svensson, and A. Yu. Kuznetsov, *Phys. Rev. Lett.* **110**, 015501 (2013).